ACS APPLIED MATERIALS & INTERFACES

Research Article

www.acsami.org

Hierarchically Porous Titania Networks with Tunable Anatase:Rutile Ratios and Their Enhanced Photocatalytic Activities

Lu Cao,[†] Dehong Chen,*[,†] Wei Li,[‡] and Rachel A. Caruso*[,†,‡]

[†]Particulate Fluids Processing Centre, School of Chemistry, The University of Melbourne, Melbourne, Victoria 3010, Australia

[‡]CSIRO Manufacturing Flagship, Private Bag 10, Clayton, Victoria 3168, Australia

Supporting Information

ABSTRACT: Mixed-phase hierarchically porous titania networks (PTNs) with 3D interconnected porous frameworks and tunable rutile contents have been synthesized via a facile sol–gel templating and calcination process. The products were characterized using scanning electron microscopy, powder X-ray diffraction, and nitrogen gas sorption analysis, and their photocatalytic activities were evaluated by measuring the photocatalytic degradation of methylene blue, a typical effluent from the textile industry, under UV light illumination. The hierarchically macro-/mesoporous titania structure formed after templating followed by calcination in air. The reduced interfaces between titania nanocrystals in these PTN materials can significantly decrease interface nucleation of the rutile phase and effectively retard the anatase to rutile phase transformation, therefore giving rise to porous titania photocatalysts featuring tunable rutile ratios (from 0 to 100 wt %), reduced crystal sizes, hierarchically porous structure, and relatively high specific surface areas (up to 71.0 m^2 g^{-1}). The photocatalytic performance of the materials was correlated to the anatase:rutile ratio and specific surface area of the materials, with the mixed-phase (rutile content of 15.4%) nanocrystalline titania calcined at 600 °C for 6 h showing the highest photocatalytic activity. This study demonstrates that a substantial improvement in photocatalytic activity of the titania can be achieved by controlling morphology and carefully tuning phase composition via a feasible solid-state phase transformation at a relatively low temperature (600 °C). This concept for the rational design and development of high-performance photocatalysts using an industrially simple process would be capable of mass production.

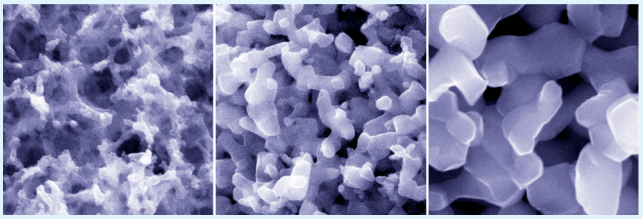

KEYWORDS: *titanium dioxide, nanostructure, porous material, phase transformation, photocatalysts, interfaces, solid-state reaction, phase junction*

INTRODUCTION

As an important industrial product, titania (TiO_2) has been widely used as an inorganic pigment, a photocatalyst, in sunscreen, sensors, energy storage and conversion devices, and electrochromics.[1−19] Because of its unique properties including superior photocatalytic activity, excellent photo- and chemical stability, nontoxicity, and relatively low cost for production, titania has been extensively studied for diverse photocatalytic applications ranging from water splitting to environmental remediation in the past several decades.[2−4,15−17,20−29] To enhance photocatalytic efficiency for practical applications, various innovative strategies, such as doping titania with diverse metal/nonmetal elements,[2,21,22,30] forming anatase–rutile mixed-phase composites,[24,31−40] creating noble metal–titania heterojunctions or coupling with narrow-band semiconductor nanoparticles (e.g., CdS/TiO_2),[41−46] and attaching titania nanocrystals to graphene nanosheets,[47−49] have been applied to optimize the performance of this photocatalyst. These modifications could effectively broaden the light absorbance of the photocatalysts,[21,22,30,47,49] promote spatial separation of photogenerated electrons and holes and therefore prevent their recombination,[35−42,44,46] facilitate electron conduction within the photocatalyst,[47,49] and thus enhance the performance of the titania photocatalyst. Among diverse strategies, forming anatase–rutile mixed-phase composites is an easy, low-cost, and scalable process, and is generally recognized as a highly practical approach for fabricating efficient titania photocatalysts for environmental remediation applications. For example, the commercially available benchmark photocatalyst, Evonik (Degussa) P25 nanoparticles,[50−53] is a mixed-phase titania with a typical anatase:rutile ratio of 80:20. Ample evidence has clearly revealed that such mixed-phase photocatalysts can significantly promote spatial separation of photogenerated electrons and holes, therefore enhancing the photocatalytic performance.[33,35−39,42,54]

Thermodynamically, rutile is the most stable phase among diverse polymorphs of titania, and anatase can be readily transformed into rutile via a solid-state phase transformation (usually by calcination at above 550 °C in air).[1,16,52] From the viewpoint of large-scale industrial production of mixed-phase titania photocatalysts, solid-state phase transformation is generally viewed as a promising process.[1,16,52] However, some

Received: May 14, 2014
Accepted: July 23, 2014
Published: August 4, 2014

obstacles still remain: (1) exaggerated grain growth of rutile crystals usually occurs with the anatase to rutile phase transformation due to the increased mobility of atoms and the heat released during the phase transformation;[52,55,56] and (2) unavoidable titania agglomerations form when sintered at elevated temperature,[52,53] and this gives rise to photocatalysts with significantly reduced specific surface area and porosity, therefore resulting in limited effectiveness in practical applications.

The phase transformation process from anatase to rutile has been extensively studied for both scientific and technological interest because crystal phase is an important factor in determining properties of titania. In general, this solid-state phase transformation proceeds via a nucleation and growth process, and three nucleation modes, interface-, surface-, and bulk-nucleation,[52,57−63] have been proposed to illustrate the anatase to rutile phase transformation. The predominant nucleation mode in a typical solid-state reaction highly depends on the calcination temperature, packing characteristic, and other physical properties of the precursors.[32,58,59,61,64] Interface-nucleation usually triggers and governs the phase transformation at a relatively low temperature (e.g., <620 °C); in contrast, a very high calcination temperature (e.g., >1000 °C) would induce the bulk-nucleation process by initializing a strong thermal fluctuation of the Ti and O atoms in anatase, and the phase transformation is usually accomplished in a short period (several minutes). For the phase transformation conducted at an intermediate temperature, it usually proceeds predominantly via a surface-nucleation process. Of these three nucleation modes, the interface-nucleation process can occur and proceed at a relatively low calcination temperature,[61] which could help to inhibit a fast growth of rutile nanocrystals. As a result, a relatively high specific surface area can be retained in the final products, which would generally enhance the effectiveness of the photocatalyst by increasing active sites available for reaction.

Besides calcination temperature, the interfaces between titania nanocrystals have been demonstrated to be another important factor in affecting the kinetics of the anatase to rutile phase transformation.[58,59,64,65] As reported by Banfield et al. and other researchers,[58,59,63,66] the anatase twin boundaries constructed from two slabs of octahedral zigzag chains have structural similarity to those of the rutile phase.[59,66] Such anatase twin interfaces can act as nuclei for the rutile phase, thus initializing the phase transformation due to their relatively low activation barriers for nucleation, in comparison to either surface- or bulk-nucleation involving an energy-intensive high temperature process.[54,59] Therefore, a reduction in anatase−anatase interface can slow the phase transformation, especially when this transformation is governed by the interface nucleation mode, which can proceed at a relatively low calcination temperature. This gives another variable to control the kinetics of phase transformation and to tailor the properties of the products.

Herein, a hierarchically porous titania network (PTN) composed of nanoparticles was prepared via a facile sol−gel templating process and employed as the precursor for fabricating mixed-phase titania photocatalysts featuring hierarchically porous structure, tunable rutile ratio, and relatively high specific surface area. As compared to conventional titania aggregates (illustrated in Scheme 1a), such PTN materials possess substantially reduced nanocrystal interfaces (Scheme 1b). This can significantly decrease interface nucleation of the rutile phase and effectively retard the phase transformation at a relatively low temperature (600 °C), therefore giving rise to porous titania photocatalysts with optimized rutile ratios and relatively high specific surface areas simply by varying calcination duration. Photocatalytic activities of the PTN with different percentages of rutile phase and specific surface areas were tested by monitoring the photodegradation of methylene blue under UV light illumination. A comparative study of photocatalytic activities of the control samples prepared in the absence of templates (macropores) was also conducted to clarify the underlying mechanism of the enhanced photocatalytic performance of the PTN materials.

Scheme 1. An Illustration of the Anatase to Rutile Phase Transformation in (a) Titania Aggregates with Abundant Interfaces (Highlighted as Red Lines) between Nanocrystals, and in (b) Porous Titania Networks with Much Reduced Interfaces[a]

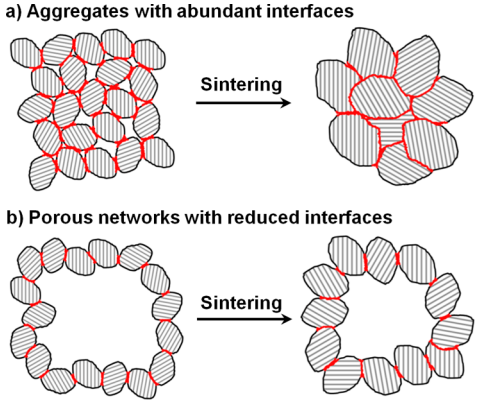

[a]A reduction in interface between nanocrystals can significantly decrease interface nucleation of the rutile phase and effectively retard the phase transformation at a relatively low temperature (e.g., 600 °C), therefore giving rise to porous titania networks featuring tunable rutile content, reduced crystal sizes, hierarchically porous structure, and relatively high specific surface areas.

EXPERIMENTAL SECTION

Chemicals. All chemical reagents were commercial products and were used without further purification. The porous agarose gel template was prepared using an agarose powder (molecular biology grade) from Scientifix. The metal alkoxide precursor, titanium(IV) isopropoxide (TIP; 97%), was purchased from Sigma-Aldrich. The isopropanol (99.5%) and ethanol (99.5%) solvents were purchased from Chem-Supply. The methylene blue (MB) used to illustrate photodegradation performance was from BDH Chemical Ltd. The Milli-Q water used in the experiment was collected on a Millipore Academic A10 purification system and had a resistivity no less than 18.2 MΩ cm.

Preparation of Agarose Gel Template. A procedure as previously detailed was employed for the preparation of a porous 1 wt % agarose gel template.[67] In brief, agarose powder (2 g) was added slowly to 198 mL of water within a beaker under stirring at room temperature. The resulting suspension was heated until a clear solution was obtained. This clear solution was then immediately poured into Pyrex test tubes and sealed with Parafilm. The test tubes were left at room temperature overnight to allow for complete gelation.

Preparation of Hierarchically Porous Titania Networks. The agarose gels were cut into small pieces (~3 × 5 × 5 mm^3) and underwent a solvent exchange from water to ethanol in three steps (water-to-ethanol volume ratio of 2:1, 1:2, then 0:1, soaking for 6 h in each solution), and similarly from ethanol to isopropanol. Subsequently, the gel pieces were soaked in 70 wt % TIP in isopropanol

solution for 18 h, before being transferred into water/isopropanol (1:1 v/v) mixed solvent for hydrolysis and condensation reactions. After 18 h, the samples were removed from solution and dried at room temperature in the fume hood for 3 days. These air-dried samples were calcined at various temperatures (500, 550, 600, 650, 700, 800, or 900 °C) for 2 h under flowing air with a ramp rate of 1.6 °C min^{-1}. To investigate the effect of prolonged calcination time, the samples were calcined at 600 °C for different durations (2, 6, 10, or 24 h). The resulting hierarchically PTN samples were labeled as PTN-*x*C-yh, where *x* indicates calcination temperature (°C) and *y* is the duration (h). For instance, PTN-600C-2h refers to the resultant porous titania calcined at 600 °C for 2 h in air. The same sol–gel synthesis (18.1 mL of 70 wt % TIP added to a mixture of 125 mL of water and 125 mL of isopropanol) and calcination procedure was employed to prepare the control samples in the absence of agarose gel templates. In this case, the control samples were denoted as Control-*x*C-*y*h.

Characterization. The morphology and average grain size of the samples were observed using a field emission environmental scanning electron microscope (FEI Quanta 200F). The samples were observed without metal sputter coating. Powder X-ray diffraction (XRD, Philips PW1800 diffractometer with Cu Kα radiation) was used to determine the crystalline phase and to estimate the rutile phase content and crystal size of the resulting titania materials. The diffractometer was set at 40 kV accelerating voltage and 20 mA applied current, and the samples were scanned from 10° to 80° at a rate of 0.02° s^{-1}. The obtained patterns were then utilized to determine weight percentage of the rutile phase titania, using the following equation:[62]

$$W_R\,(\%) = 100A_R/(0.886A_A + A_R + 2.721A_B)$$

where A_A, A_R, and A_B represent the integrated intensities of the anatase (101), rutile (110), and brookite (121) peaks, respectively. Nitrogen gas sorption isotherms were measured at −196 °C by the volumetric method on a Micromeritics Tristar 3000 surface area and porosity analyzer. Prior to the measurement, samples were evacuated at 150 °C for 18 h on a vacuum line (less than 30 mTorr). The standard multipoint Brunauer–Emmett–Teller (BET) method was utilized to calculate the specific surface area using the adsorption data in the P/P_0 range from 0.05 to 0.20. The pore size distributions of the materials were derived from the adsorption branches of the isotherms on the basis of the Barett–Joyner–Halenda (BJH) model.

Photocatalytic Activity. Photocatalytic activities of the PTN (40 mg) and the control samples (40 mg) were studied by monitoring the degradation of MB (80 mL, 55.5 mg L^{-1}) in an aqueous solution under UV irradiation with continuous magnetic stirring. Before irradiation, the suspension was equilibrated in a jacketed beaker by stirring in the dark for 1 h to equilibrate the adsorption of MB dye onto the surface of titania. The jacketed beaker was kept at 20 ± 0.5 °C with chilled water running through a thermostatic circulated bath. The MB solution was continuously bubbled with air (industrial grade, BOC) during stabilization and degradation. A 500 W Hg (Xe) globe (Oriel) with a dichroic mirror (66226, Oriel, 280 < λ < 400 nm) was used to deliver light vertically through a quartz reactor lid. Following UV-radiation exposure, the degradation of the MB dye was monitored by taking 1.5 mL aliquots at regular irradiation intervals (0, 15, 30, 45, and 60 min). These aliquots were centrifuged at 15 000 rpm for 10 min to separate the catalyst from the mixture. The supernatants were collected and analyzed by recording the characteristic absorption peak of MB (664 nm) using a UV–vis spectrophotometer (Varian Cary 50 Bio).

RESULTS AND DISCUSSION

Morphological Evolution of the PTN and Control Samples. Both the temperature during calcination treatment and the nanoparticle packing characteristics in the precursor materials play crucial roles in influencing the morphologies of the final titania materials. Figure 1 shows SEM images of both PTN and control samples obtained by calcining the titania/agarose composite and titania at temperatures ranging from 500 to 800 °C. PTN materials calcined at 500 °C (Figure 1a,b and Figure S1a in the Supporting Information) consist of titania nanocrystals <10 nm in diameter and show a hierarchically porous framework containing interconnected macropores ranging from 80 to 200 nm in diameter. After calcination at 600 °C (Figure 1c and Supporting Information Figure S1b), the macroporous structure was retained in the PTN material, and slightly enlarged titania crystals were observed. In contrast, the control sample (Figure 1d) fabricated in the absence of agarose gel templates formed a compact aggregate consisting of ~35 nm titania nanocrystals. Increasing the calcination temperature to 700 °C (Figure 1e and Supporting Information Figure S1c) or 800 °C (Figure 1g and Supporting Information Figure S1d) resulted in the PTN material becoming more "compact", mainly due to shrinkage of the inorganic framework along with the coarsening of the titania crystals (diameters up to 170 nm after being heated at 800 °C). As clearly illustrated in Figure 1f and h, at such high temperatures (>700 °C) the control samples show densely sintered and relatively large titania crystals (~170 nm at 700 °C and ~260 nm at 800 °C). The crystal size of the control samples is much larger than that in the PTN materials synthesized in the presence of agarose gel templates when calcined at 700 °C or above. Increasing the calcination temperature to 900 °C gave uniform PTN materials (Supporting Information Figure S2a,b) featuring 3D interconnected frameworks and faceted rutile crystals (Supporting Information Figure S3) ranging from 120 to 450 nm in size (Supporting Information Figure S2c,d), showing a significant growth in crystal size.

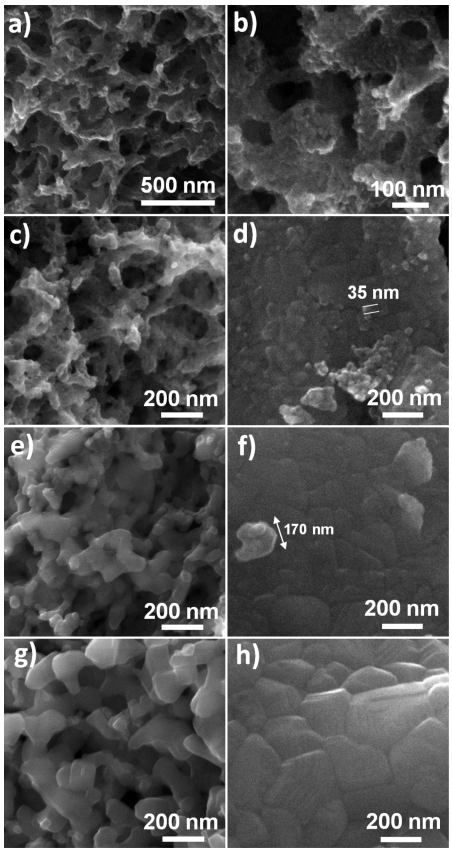

Figure 1. SEM images of the porous titania networks (a, b, c, e, and g) and control samples (d, f, and h) sintered at (a, b) 500 °C, (c, d) 600 °C, (e, f) 700 °C, and (g, h) 800 °C for 2 h in air. Note: All of these images were obtained without metal sputter coating of the samples.

As both the PTN and the control samples were prepared via an identical sol–gel reaction and calcination process, the above results clearly reveal that the reduced interfaces between titania nanocrystals can effectively retard crystal growth in the PTN materials.

The effect of the calcination time on the evolution of such PTN nanostructures was also investigated. Figure 2 shows SEM images of the PTN samples sintered at 600 °C for 2–24 h in air, and no obvious differences in the inorganic frameworks were observed for these PTN samples.

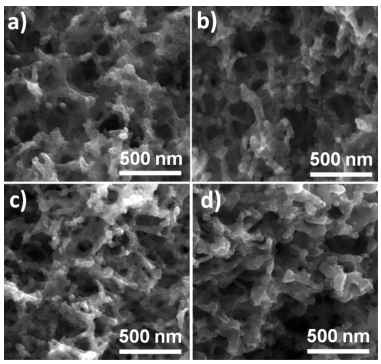

Figure 2. SEM images of the porous titania networks sintered at 600 °C for (a) 2 h, (b) 6 h, (c) 10 h, and (d) 24 h in air. Note: All of these images were obtained without metal sputter coating of the samples.

Crystal Phase Transformation and Rutile Content. The changes in crystal phase and crystallite size within the PTN and control samples were studied by powder X-ray diffraction (XRD), and the corresponding patterns of the samples calcined at different temperatures are presented in Figure 3. Rutile contents (weight percentages) in each sample were calculated according to a previously reported method,[62] and the corresponding results are listed in Table 1. There was no rutile diffraction peak observed in either the PTN sample or the control sample calcined at 500 °C (Figure 3a,b). After calcination at 550 °C for 2 h, a small peak at 2θ = 27.4° (Supporting Information Figure S5), corresponding to the (110) plane of the rutile phase titania, appeared in both the PTN and the control samples, indicating the occurrence of phase transformation from anatase to rutile at this temperature. This result is in good agreement with those reported previously.[52,55] After calcination at 550 °C for 2 h, the rutile content of the PTN-550C-2h and Control-550C-2h sample was 5.8% and 9.3%, respectively. When the calcination temperature increased to 600 °C, the amount of rutile increased slightly to 11.7%; see the PTN-600C-2h sample. This is substantially different to the Control-600C-2h sample, where the intensity of the anatase diffraction peaks decreased significantly and the intensity of the rutile diffraction peaks increased sharply (as compared to the Control-550C-2h) and that was 80.0% rutile phase. Additionally, the crystallite size of the anatase in this control sample increased drastically to 35 nm because the heat of phase transformation from anatase to rutile accelerated grain growth.[55,56] In comparison with this control sample, only a slight increase in crystallite size was observed when calcining the PTN at 600 °C (Figure 1c and Supporting Information Figure S1b, PTN-600C-2h). With a further increase in the calcination temperature, the control sample was fully converted to the rutile phase at 800 °C, while the PTN material retained 12.6% anatase at 800 °C. As summarized in Figure 4, the anatase-to-rutile phase transformation was significantly retarded in the PTN materials, especially when the calcination temperature is below 650 °C, at which an interface nucleation mechanism dominates the anatase to rutile phase transformation.[61]

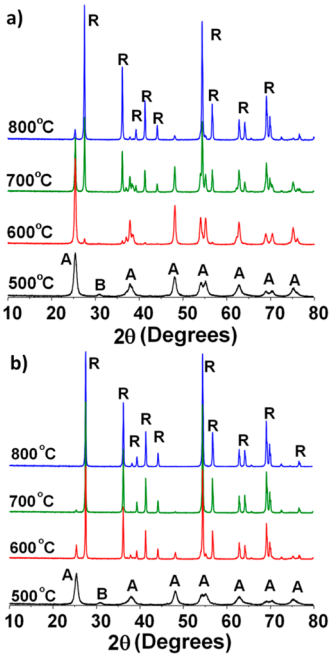

Figure 3. XRD patterns of (a) the porous titania networks and (b) control samples sintered at diverse temperatures (as noted on the individual patterns) for 2 h in air. A = anatase, B = brookite, and R = rutile titania.

Rutile contents in the PTN materials were tunable by changing calcination time as well. The PTN materials calcined at 600 °C for 2, 6, 10, and 24 h were investigated and characterized using XRD. The corresponding XRD patterns are shown as Supporting Information Figure S6, and physical properties are given in Table 1. The rutile percentage increased from 11.7 to 28.4 wt % when the calcination time was prolonged from 2 to 24 h (Table 1). Even with this prolonged calcination of 24 h, the rutile content was significantly less (28.4% for PTN-600C-24h) than that of the Control-600C-2h (80.0%) sample calcined for 2 h at the same temperature. On the basis of the above results, it is clear that the presence of the agarose gel template during sol–gel synthesis gave rise to a hierarchically porous structure that effectively reduces the interfaces between titania nanocrystals, and therefore prevented phase transformation by inhibiting nucleation of the rutile phase. Thus, controlling calcination temperature or duration at a relatively low temperature (e.g., 600 °C) renders a facile and feasible method to tune anatase to rutile ratios and adjust titania crystal sizes in the PTN materials.

Specific Surface Area and Porosity of the PTN and Control Samples. To explore the correlation between porous structure and phase transformation, and the effects of pores on photocatalytic performance, specific surface areas and pore size distributions of the PTN and control samples calcined at varying temperatures and times were characterized using nitrogen gas sorption. Specific surface areas of the PTN and control samples as a function of calcination temperature from 500 to 900 °C are given in Figure 5. For the control sample

Table 1. Physical Properties of the Porous Titania Networks (PTN) and Control Samples

sample	crystal phase[a]	W_R (wt %)[b]	surface area (m^2 g^{-1})[c]	relative surface area (%)[d]	pore diameter (nm)[e]	pore volume (cm^3 g^{-1})[f]
PTN-500C-2h	A + B	0.0	71.0 ± 1.0	100	14.9, 90	0.248
PTN-550C-2h	A + B + R	5.8	52.2 ± 0.5	73.5	14.7, 98	0.211
PTN-600C-2h	A + R	11.7	36.6 ± 0.4	51.5	16.0, 92	0.125
PTN-650C-2h	A + R	24.0	24.4 ± 0.3	34.4	16.0, 96	0.115
PTN-700C-2h	A + R	54.5	17.0 ± 0.3	23.9	102	0.112
PTN-800C-2h	A + R	87.4	10.7 ± 0.2	15.1	105	0.042
PTN-900C-2h	R	100	5.0 ± 0.2	7.0	158	0.034
PTN-600C-2h	A + R	11.7	36.6 ± 0.4	51.5	16.0, 92	0.125
PTN-600C-6h	A + R	15.4	32.2 ± 0.4	45.4	16.8, 80	0.122
PTN-600C-10h	A + R	17.3	28.2 ± 0.3	39.7	17.0, 78	0.117
PTN-600C-24h	A + R	28.4	21.9 ± 0.3	30.8	75	0.090
Control-500C-2h	A + B	0.0	92.5 ± 0.9	100	6.0	0.237
Control-550C-2h	A + B + R	9.3	34.3 ± 0.4	37.1	8.5	0.133
Control-600C-2h	A + R	80.0	4.9 ± 0.2	0.05		0.069
Control-700C-2h	A + R	91.8	3.2 ± 0.1	0.03		0.064
Control-800C-2h	R	100	2.4 ± 0.1	0.03		0.044

[a]Crystal phase of the samples determined using XRD technique, A = anatase, R = rutile, and B = brookite titania. [b]Weight percentage of the rutile titania calculated using the integrated intensities of anatase (101), rutile (110), and brookite (121) peaks according to a previously reported method.[62] [c]Specific surface area calculated from nitrogen gas adsorption data in the P/P_0 range from 0.05 to 0.20. [d]Relative specific surface area, normalized to PTN-500C-2h for PTN samples and to Control-500C-2h for control samples, respectively. [e]Pore diameter determined by the BJH model using the nitrogen adsorption branch data. [f]Cumulative volume of pores between 1.70 and 300 nm calculated from the nitrogen adsorption data.

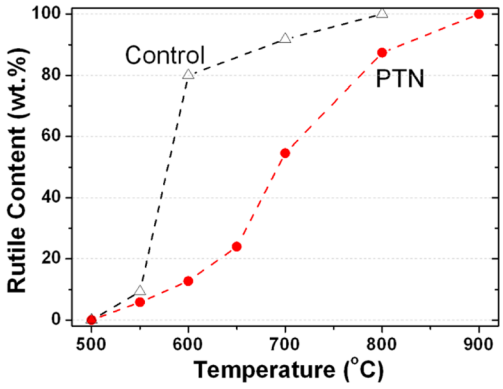

Figure 4. Rutile content of the porous titania networks (PTN) and control samples (Control) calculated from the corresponding XRD patterns. The dashed lines were added to guide the eye.

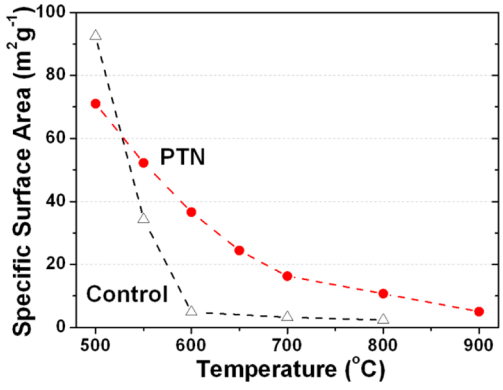

Figure 5. Specific surface areas of the porous titania networks (PTN) and control samples (Control) as a function of the calcination temperature from 500 to 900 °C. The dashed lines were added to guide the eye.

calcined at 500 °C for 2 h, the specific surface area (92.5 m^2 g^{-1}) was higher than that of the PTN material prepared under the same calcination condition, PTN-500C-2h (71.0 m^2 g^{-1}). However, the specific surface area of the control samples dropped dramatically to 4.9 m^2 g^{-1} (Table 1) by increasing the calcination temperature to 600 °C. In contrast, the specific surface area of the PTN samples decreased gradually to 36.6 m^2g^{-1} at 600 °C, and then to 10.7 m^2 g^{-1} after calcination at 800 °C for 2 h, indicating the higher thermal stability of the PTN materials. The specific surface areas of the PTN materials calcined at 600 °C for various times were also investigated and dropped gradually from 36.6 to 21.9 m^2 g^{-1} with a calcination time from 2 to 24 h (Supporting Information Figure S7). As demonstrated in the SEM images (Figures 1 and 2) and XRD patterns (Figure 3), hierarchically porous frameworks and relatively small crystal sizes can be effectively retained in the PTN materials while increasing calcination temperature and duration; thus a relatively high specific surface area can be obtained in the PTN materials (Table 1).

Nitrogen gas sorption isotherms of the PTN materials calcined at various temperatures are shown in Figure 6a. Except for the PTN-800C-2h sample, all of the isotherms showed two hysteresis loops at relative pressures (P/P_0) ranging from 0.65 to 0.96, indicating a bimodal pore size distribution (presence of both mesopores and macropores).[68] The macropores were a result of the templating process, where the coated agarose fibers, separated by hundreds of nanometers, left large voids in the final structure. These macropores in the PTN materials were preserved even when the calcination temperature was as high as 900 °C (Supporting Information Figure S2). The mesopores in the PTN materials stem from both the removal of the agarose fibrils and the interparticle voids between the titania nanocrystals. For the PTN material calcined at 500 °C for 2 h, as shown in the inset, two distinct pore size distributions centered around 14.9 and 90 nm were obtained. The abundance of mesopores decreases as the calcination temperature increases to 650 °C, while the macropore profile changes slightly from 600 to 650 °C. After calcination at 800 °C, the mesopores of the PTN material disappeared, indicating a

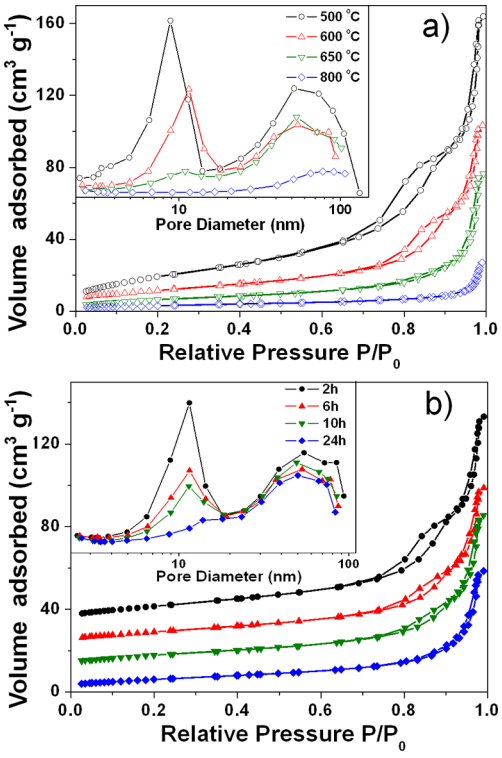

Figure 6. Nitrogen sorption isotherms and corresponding pore size distributions (insets) of the porous titania networks sintered (a) at diverse temperatures and (b) at 600 °C for varied times (from 2 to 24 h) in air.

significant crystal growth and densification of the inorganic frameworks. This can be clearly observed in the corresponding SEM images (Figure 1g and Supporting Information Figure S1d). It is worth noting that even after calcination at 900 °C, as clearly demonstrated in Supporting Information Figure S2, three-dimensional interconnected macropores remain in this PTN material, demonstrating an excellent thermal stability.

Besides the calcination temperature, the calcination duration also affects the porosity of the resulting materials. For PTN samples calcined at 600 °C for different lengths of time, as shown in Figure 6b, the mesopores gradually decreased when heated from 2 to 24 h, while only a slight decrease in the corresponding macropore profiles was observed. This varying trend in meso- and macropore profiles suggests that a gradual densification occurred mostly at the interfaces between titania nanocrystals, and this interfacial densification might proceed via the nucleation of the rutile phase located at the anatase–anatase interfaces.

Before presenting the photocatalytic results, it is instructive to discuss the relationship between porous structure and anatase-to-rutile phase transformation. According to the previous reports,[58,59,64] the packing characteristic of the titania nanocrystals has a significant effect on the crystal phase transformation. From the SEM images shown in Figure 1b, the hierarchically porous framework of the PTN samples is composed of titania nanoparticles less than 10 nm in diameter. Large porosity in such a porous structure means a decreased number of neighboring particles as compared to a dense structure (as illustrated by the control samples) and, hence, would result in a decrease in interface nucleation of the rutile phase. XRD results show that such hierarchically porous structures can effectively retard the anatase to rutile phase transformation at elevated temperatures. Employing such PTNs as parent materials, finely controllable phase transformation can be realized using a facile and feasible calcination process at an elevated temperature (e.g., 600 °C), and gives rise to PTN samples with tunable crystal phases, enhanced crystallinity, 3D interconnected porous frameworks, and relatively high specific surface areas.

Photocatalytic Performance. Photocatalytic activities of the resulting PTN materials were evaluated by the degradation of methylene blue (MB), a probe molecule, under UV light irradiation. For comparison, photocatalytic activities of the control samples (without macropores) calcined at the same temperatures were also measured under the same conditions. To compare the reaction kinetics of the MB degradation, a pseudo-first-order reaction equation, $\ln(C/C_0) = -kt$, where C_0 and C are the initial concentration and the reaction concentration of MB at an irradiation time t, respectively, and k is the apparent reaction rate constant,[28,29] was applied to the time profile of the MB absorption spectra (Figure S8 in the Supporting Information).

The calcination temperature has a great effect on the photocatalytic activities of titania materials (Figure 7a). At 500

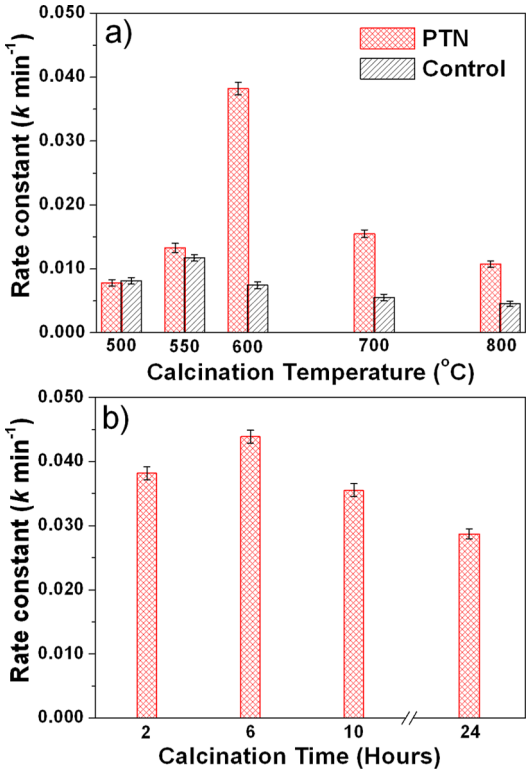

Figure 7. Comparison of the apparent rate constants in photocatalytic reactions employing (a) porous titania networks (PTN) and control samples (Control) calcined at varying temperatures for 2 h, and (b) PTN samples calcined at 600 °C for 2–24 h.

°C, the apparent reaction rate constant, k, of the PTN material is equivalent (within error) to that of the control sample. With an increase in calcination temperature to 550 °C, the degradation rate of MB increased for both the PTN and the control samples. A small amount of rutile appeared in both samples (Table 1) and is presumably the main reason for the improved photocatalytic performance. The coexistence of anatase and rutile phases can effectively inhibit the recombi-

nation of photocarriers by promoting the spatial charge separation and, therefore, enhances the efficiency of photodegradation.[8−13] Comparing the performance of these two samples, we believe that the higher surface area of the PTN-550C-2h (52.2 m^2 g^{-1}) has enhanced the photocatalytic activity. Although the specific surface area decreased with increasing calcination temperature, a sharp increase in photocatalytic activity in PTN-600C-2h (k = 0.0382 min^{-1}) was observed when the calcination temperature reached 600 °C. In contrast, a decrease in photocatalytic activity was observed for the Control-600C-2h sample, probably due to its very low specific surface area (4.9 m^2 g^{-1}) and substantial quantities of rutile (80.0 wt %) after calcination at this temperature. Increasing the temperature to 700 and 800 °C decreased the photocatalytic activities of both the PTN and the control samples as a result of the ongoing phase transformation and crystal growth, which leads to a remarkable reduction in the specific surface area (Table 1).

The effect of calcination time on photocatalytic performance of the PTN materials was also investigated, and the results are shown in Figure 7b. Although the specific surface area of the PTN materials decreased from 36.6 to 32.2 m^2 g^{-1} when increasing the calcination time from 2 to 6 h, this did not result in a decrease in the photocatalytic activity. The PTN-600C-6h sample gave the highest photocatalytic activity with an apparent reaction rate constant of 0.0439 min^{-1}. This increase in the photocatalytic activity could be attributed to the formation of more anatase/rutile phase junctions (Figure 8) and the improved crystallinity of the PTN materials.[24,28,29,36,37,39,42,53] A decrease in the photocatalytic activity was observed for calcination times of 10 h or longer when heated at 600 °C, mainly due to the decrease in reactive sites in the PTN materials as a result of the reduction in specific surface area (Table 1). On the basis of the above results, it is clear that both calcination temperature and the presence of macro-/mesopores in the parent materials play very important roles in determining the properties of the PTN materials. PTN materials with optimized rutile content (~15.4 wt %) can be obtained by annealing at a relatively low temperature (600 °C), giving enhanced photocatalytic activity due to the finely controllable anatase-to-rutile phase transformation kinetics governed by the interface nucleation process.

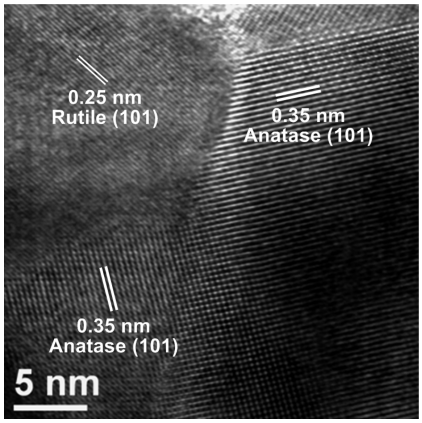

Figure 8. High-resolution TEM image of the porous titania network clearly showing the phase junctions between rutile and anatase nanocrystals.

CONCLUSIONS

Hierarchically porous titania networks with controllable rutile content and relatively high specific surface area were prepared via a facile templating and solid-state phase transformation process dominated by the interface nucleation process at a relatively low temperature (600 °C). The PTN (templated by the agarose gel) possessed reduced contact areas between titania nanocrystals and effectively suppressed the anatase to rutile phase transformation and the rutile crystal growth, thus giving rise to hierarchically porous titania photocatalysts that could be optimized for rutile content and maintain relatively high specific surface areas. Such agarose-templated PTN showed excellent thermal stability and structural homogeneity, even after being transformed into the rutile phase at 900 °C in air. The hierarchically PTN materials showed enhanced photocatalytic activity toward the degradation of methylene blue under UV light irradiation, due to optimized crystal phase composition and increased number of reactive sites (due to higher surface area), when compared to the control samples prepared in the absence of template under otherwise identical conditions. The coexistence of the anatase and rutile phases is beneficial for photocatalytic performance, relative to either individual component. This work demonstrates a facile synthesis method for fabricating tunable mixed-phase titania materials with improved photocatalytic activity. Given their hierarchically porous structures, robust inorganic frameworks, tunable anatase:rutile ratios, and relatively high specific surface areas, the resultant PTN materials are expected to find potential applications in the area of industrial oxidation catalysis.

ASSOCIATED CONTENT

Supporting Information

SEM images, XRD patterns, and rutile content of the PTN materials fabricated at varying calcination temperatures (from 500 to 900 °C) and durations (from 2 to 24 h) and photocatalytic degradation performance of both the PTN and the control samples. This material is available free of charge via the Internet at http://pubs.acs.org.

AUTHOR INFORMATION

Corresponding Authors

*Tel.: 61 3 8344 7146. Fax: 61 3 9347 5180. E-mail: rcaruso@unimelb.edu.au.

*E-mail: dehongc@unimelb.edu.au.

Notes

The authors declare no competing financial interest.

ACKNOWLEDGMENTS

This research was financially supported by an Australian Research Council Discovery Project (DP110101346). L.C. acknowledges the support of an Australian Postgraduate Award and MMI-CSIRO Ph.D. Materials Science Top-up. R.A.C. is a recipient of an Australian Research Council Future Fellowship (FT0990583). The Melbourne Advanced Microscopy Facility of The University of Melbourne is acknowledged for electron microscopy access.

REFERENCES

(1) Winkler, J. *Titanium Dioxide: Production, Properties and Effective Usage*; Vincentz Network: Hanover, Germany, 2013.

(2) Chen, X.; Mao, S. S. Titanium Dioxide Nanomaterials: Synthesis, Properties, Modifications, and Applications. *Chem. Rev.* **2007**, *107*, 2891−2959.
(3) Fujishima, A.; Zhang, X. T.; Tryk, D. A. TiO_2 Photocatalysis and Related Surface Phenomena. *Surf. Sci. Rep.* **2008**, *63*, 515−582.
(4) Fujishima, A.; Hashimoto, K.; Watanabe, T. *TiO_2 Photocatalysis: Fundamentals and Applications*; BKC, Inc.: Tokyo, Japan, 1999.
(5) Fujishima, A.; Honda, K. Electrochemical Photolysis of Water at a Semiconductor Electrode. *Nature* **1972**, *238*, 37−38.
(6) Grtäzel, M. Photoelectrochemical Cells. *Nature* **2001**, *414*, 338−344.
(7) Sauvage, F.; Chen, D. H.; Comte, P.; Huang, F. Z.; Heiniger, L. P.; Cheng, Y. B.; Caruso, R. A.; Graetzel, M. Dye-Sensitized Solar Cells Employing a Single Film of Mesoporous TiO_2 Beads Achieve Power Conversion Efficiencies over 10%. *ACS Nano* **2010**, *4*, 4420−4425.
(8) Chen, Z.; Belharouak, I.; Sun, Y. K.; Amine, K. Titanium-Based Anode Materials for Safe Lithium-Ion Batteries. *Adv. Funct. Mater.* **2013**, *23*, 959−969.
(9) Chen, D. H.; Huang, F. Z.; Cao, L.; Cheng, Y. B.; Caruso, R. A. Spiky Mesoporous Anatase Titania Beads: A Metastable Ammonium Titanate Mediated Synthesis. *Chem.—Eur. J.* **2012**, *18*, 13762−13769.
(10) Zhu, G. N.; Wang, Y. G.; Xia, Y. Y. Ti-Based Compounds as Anode Materials for Li-Ion Batteries. *Energy Environ. Sci.* **2012**, *5*, 6652−6667.
(11) Wagemaker, M.; Kentgens, A. P. M.; Mulder, F. M. Equilibrium Lithium Transport between Nanocrystalline Phases in Intercalated TiO_2 Anatase. *Nature* **2002**, *418*, 397−399.
(12) Chen, D. H.; Caruso, R. A. Recent Progress in the Synthesis of Spherical Titania Nanostructures and Their Applications. *Adv. Funct. Mater.* **2013**, *23*, 1356−1374.
(13) Enache, D. I.; Edwards, J. K.; Landon, P.; Solsona-Espriu, B.; Carley, A. F.; Herzing, A. A.; Watanabe, M.; Kiely, C. J.; Knight, D. W.; Hutchings, G. J. Solvent-Free Oxidation of Primary Alcohols to Aldehydes Using Au-Pd/TiO_2 Catalysts. *Science* **2006**, *311*, 362−365.
(14) Chen, D. H.; Huang, F. Z.; Cheng, Y. B.; Caruso, R. A. Mesoporous Anatase TiO_2 Beads with High Surface Areas and Controllable Pore Sizes: A Superior Candidate for High-Performance Dye-Sensitized Solar Cells. *Adv. Mater.* **2009**, *21*, 2206−2210.
(15) Linsebigler, A. L.; Lu, G. Q.; Yates, J. T. Photocatalysis on TiO_2 Surfaces - Principles, Mechanisms, and Selected Results. *Chem. Rev.* **1995**, *95*, 735−758.
(16) Carp, O.; Huisman, C. L.; Reller, A. Photoinduced Reactivity of Titanium Dioxide. *Prog. Solid State Chem.* **2004**, *32*, 33−177.
(17) Anpo, M.; Kamat, P. V. *Environmentally Benign Photocatalysts: Applications of Titanium Oxide-Based Materials*; Springer: New York, 2010.
(18) Huang, F. Z.; Chen, D. H.; Li, Q.; Caruso, R. A.; Cheng, Y. B. Construction of Nanostructured Electrodes on Flexible Substrates Using Pre-Treated Building Blocks. *Appl. Phys. Lett.* **2012**, *100*, 123102.
(19) Chen, Y.; Huang, F. Z.; Chen, D. H.; Cao, L.; Zhang, X. L.; Caruso, R. A.; Cheng, Y. B. Effect of Mesoporous TiO_2 Bead Diameter in Working Electrodes on the Efficiency of Dye-Sensitized Solar Cells. *ChemSusChem* **2011**, *4*, 1498−1503.
(20) Hashimoto, K.; Irie, H.; Fujishima, A. TiO_2 Photocatalysis: A Historical Overview and Future Prospects. *Jpn. J. Appl. Phys.* **2005**, *44*, 8269−8285.
(21) Asahi, R.; Morikawa, T.; Ohwaki, T.; Aoki, K.; Taga, Y. Visible-Light Photocatalysis in Nitrogen-Doped Titanium Oxides. *Science* **2001**, *293*, 269−271.
(22) Chen, X. B.; Liu, L.; Yu, P. Y.; Mao, S. S. Increasing Solar Absorption for Photocatalysis with Black Hydrogenated Titanium Dioxide Nanocrystals. *Science* **2011**, *331*, 746−750.
(23) Cao, L.; Chen, D. H.; Caruso, R. A. Surface-Metastable Phase-Initiated Seeding and Ostwald Ripening: A Facile Fluorine-Free Process Towards Spherical Fluffy Core/Shell, Yolk/Shell, and Hollow Anatase Nanostructures. *Angew. Chem., Int. Ed.* **2013**, *52*, 10986−10991.
(24) Zhang, J.; Xu, Q.; Feng, Z.; Li, M.; Li, C. Importance of the Relationship between Surface Phases and Photocatalytic Activity of TiO_2. *Angew. Chem., Int. Ed.* **2008**, *47*, 1766−1769.
(25) Hoffmann, M. R.; Martin, S. T.; Choi, W. Y.; Bahnemann, D. W. Environmental Applications of Semiconductor Photocatalysis. *Chem. Rev.* **1995**, *95*, 69−96.
(26) Li, H. X.; Bian, Z. F.; Zhu, J.; Zhang, D. Q.; Li, G. S.; Huo, Y. N.; Li, H.; Lu, Y. F. Mesoporous Titania Spheres with Tunable Chamber Stucture and Enhanced Photocatalytic Activity. *J. Am. Chem. Soc.* **2007**, *129*, 8406−8407.
(27) Yang, H. G.; Sun, C. H.; Qiao, S. Z.; Zou, J.; Liu, G.; Smith, S. C.; Cheng, H. M.; Lu, G. Q. Anatase TiO_2 Single Crystals with a Large Percentage of Reactive Facets. *Nature* **2008**, *453*, 638−641.
(28) Joo, J. B.; Zhang, Q.; Dahl, M.; Lee, I.; Goebl, J.; Zaera, F.; Yin, Y. D. Control of the Nanoscale Crystallinity in Mesoporous TiO_2 Shells for Enhanced Photocatalytic Activity. *Energy Environ. Sci.* **2012**, *5*, 6321−6327.
(29) Joo, J. B.; Lee, I.; Dahl, M.; Moon, G. D.; Zaera, F.; Yin, Y. D. Controllable Synthesis of Mesoporous TiO_2 Hollow Shells: Toward an Efficient Photocatalyst. *Adv. Funct. Mater.* **2013**, *23*, 4246−4254.
(30) Wang, X. H.; Li, J. G.; Kamiyama, H.; Katada, M.; Ohashi, N.; Moriyoshi, Y.; Ishigaki, T. Pyrogenic Iron(III)-Doped TiO_2 Nanopowders Synthesized in RF Thermal Plasma: Phase Formation, Defect Structure, Band Gap, and Magnetic Properties. *J. Am. Chem. Soc.* **2005**, *127*, 10982−10990.
(31) Zhang, J.; Li, M. J.; Feng, Z. C.; Chen, J.; Li, C. UV Raman Spectroscopic Study on TiO_2. I. Phase Transformation at the Surface and in the Bulk. *J. Phys. Chem. B* **2006**, *110*, 927−935.
(32) Zhang, J.; Xu, Q.; Li, M. J.; Feng, Z. C.; Li, C. UV Raman Spectroscopic Study on TiO_2. II. Effect of Nanoparticle Size on the Outer/Inner Phase Transformations. *J. Phys. Chem. C* **2009**, *113*, 1698−1704.
(33) Su, R.; Bechstein, R.; Sø, L.; Vang, R. T.; Sillassen, M.; Esbjörnsson, B.; Palmqvist, A.; Besenbacher, F. How the Anatase-to-Rutile Ratio Influences the Photoreactivity of TiO_2. *J. Phys. Chem. C* **2011**, *115*, 24287−24292.
(34) Zachariah, A.; Baiju, K. V.; Shukla, S.; Deepa, K. S.; James, J.; Warrier, K. G. K. Synergistic Effect in Photocatalysis as Observed for Mixed-Phase Nanocrystalline Titania Processed Via Sol-Gel Solvent Mixing and Calcination. *J. Phys. Chem. C* **2008**, *112*, 11345−11356.
(35) Scanlon, D. O.; Dunnill, C. W.; Buckeridge, J.; Shevlin, S. A.; Logsdail, A. J.; Woodley, S. M.; Catlow, C. R. A.; Powell, M. J.; Palgrave, R. G.; Parkin, I. P.; Watson, G. W.; Keal, T. W.; Sherwood, P.; Walsh, A.; Sokol, A. A. Band Alignment of Rutile and Anatase TiO_2. *Nat. Mater.* **2013**, *12*, 798−801.
(36) Kawahara, T.; Konishi, Y.; Tada, H.; Tohge, N.; Nishii, J.; Ito, S. A Patterned TiO_2(Anatase)/TiO_2(Rutile) Bilayer-Type Photocatalyst: Effect of the Anatase/Rutile Junction on the Photocatalytic Activity. *Angew. Chem., Int. Ed.* **2002**, *114*, 2935−2937.
(37) Miyagi, T.; Kamei, M.; Mitsuhashi, T.; Ishigaki, T.; Yamazaki, A. Charge Separation at the Rutile/Anatase Interface: A Dominant Factor of Photocatalytic Activity. *Chem. Phys. Lett.* **2004**, *390*, 399−402.
(38) Hurum, D. C.; Agrios, A. G.; Gray, K. A.; Rajh, T.; Thurnauer, M. C. Explaining the Enhanced Photocatalytic Activity of Degussa P25 Mixed-Phase TiO_2 Using EPR. *J. Phys. Chem. B* **2003**, *107*, 4545−4549.
(39) Li, G.; Dimitrijevic, N. M.; Chen, L.; Nichols, J. M.; Rajh, T.; Gray, K. A. The Important Role of Tetrahedral Ti^{4+} Sites in the Phase Transformation and Photocatalytic Activity of TiO_2 Nanocomposites. *J. Am. Chem. Soc.* **2008**, *130*, 5402−5403.
(40) Kho, Y. K.; Iwase, A.; Teoh, W. Y.; Mädler, L.; Kudo, A.; Amal, R. Photocatalytic H_2 Evolution over TiO_2 Nanoparticles. The Synergistic Effect of Anatase and Rutile. *J. Phys. Chem. C* **2010**, *114*, 2821−2829.
(41) Tsukamoto, D.; Shiraishi, Y.; Sugano, Y.; Ichikawa, S.; Tanaka, S.; Hirai, T. Gold Nanoparticles Located at the Interface of Anatase/Rutile TiO_2 Particles as Active Plasmonic Photocatalysts for Aerobic Oxidation. *J. Am. Chem. Soc.* **2012**, *134*, 6309−6315.

(42) Li, G.; Gray, K. A. The Solid−Solid Interface: Explaining the High and Unique Photocatalytic Reactivity of TiO_2-Based Nanocomposite Materials. *Chem. Phys.* **2007**, *339*, 173−187.
(43) Wang, X. D.; Mitchell, D. R. G.; Prince, K.; Atanacio, A. J.; Caruso, R. A. Gold Nanoparticle Incorporation into Porous Titania Networks Using an Agarose Gel Templating Technique for Photocatalytic Applications. *Chem. Mater.* **2008**, *20*, 3917−3926.
(44) Subramanian, V.; Wolf, E. E.; Kamat, P. V. Catalysis with TiO_2/Gold Nanocomposites. Effect of Metal Particle Size on the Fermi Level Equilibration. *J. Am. Chem. Soc.* **2004**, *126*, 4943−4950.
(45) Tian, Y.; Tatsuma, T. Mechanisms and Applications of Plasmon-Induced Charge Separation at TiO_2 Films Loaded with Gold Nanoparticles. *J. Am. Chem. Soc.* **2005**, *127*, 7632−7637.
(46) Lakshminarasimhan, N.; Bae, E.; Choi, W. Enhanced Photocatalytic Production of H_2 on Mesoporous TiO_2 Prepared by Template-Free Method: Role of Interparticle Charge Transfer. *J. Phys. Chem. C* **2007**, *111*, 15244−15250.
(47) Lee, J. S.; You, K. H.; Park, C. B. Highly Photoactive, Low Bandgap TiO_2 Nanoparticles Wrapped by Graphene. *Adv. Mater.* **2012**, *24*, 1084−1088.
(48) Xiang, Q.; Yu, J.; Jaroniec, M. Synergetic Effect of MoS_2 and Graphene as Cocatalysts for Enhanced Photocatalytic H_2 Production Activity of TiO_2 Nanoparticles. *J. Am. Chem. Soc.* **2012**, *134*, 6575−6578.
(49) Zhang, H.; Lv, X.; Li, Y.; Wang, Y.; Li, J. P25-Graphene Composite as a High Performance Photocatalyst. *ACS Nano* **2009**, *4*, 380−386.
(50) Ohno, T.; Sarukawa, K.; Tokieda, K.; Matsumura, M. Morphology of a TiO_2 Photocatalyst (Degussa, P-25) Consisting of Anatase and Rutile Crystalline Phases. *J. Catal.* **2001**, *203*, 82−86.
(51) Bickley, R. I.; Gonzalezcarreno, T.; Lees, J. S.; Palmisano, L.; Tilley, R. J. D. A Structural Investigation of Titanium-Dioxide Photocatalysts. *J. Solid State Chem.* **1991**, *92*, 178−190.
(52) Hanaor, D.; Sorrell, C. Review of the Anatase to Rutile Phase Transformation. *J. Mater. Sci.* **2011**, *46*, 855−874.
(53) Porter, J. F.; Li, Y. G.; Chan, C. K. The Effect of Calcination on the Microstructural Characteristics and Photoreactivity of Degussa P-25 TiO_2. *J. Mater. Sci.* **1999**, *34*, 1523−1531.
(54) Wu, C.; Yue, Y.; Deng, X.; Hua, W.; Gao, Z. Investigation on the Synergetic Effect between Anatase and Rutile Nanoparticles in Gas-Phase Photocatalytic Oxidations. *Catal. Today* **2004**, *93*−*95*, 863−869.
(55) Kumar, K. N. P.; Keizer, K.; Burggraaf, A. J.; Okubo, T.; Nagamoto, H.; Morooka, S. Densification of Nanostructured Titania Assisted by a Phase-Transformation. *Nature* **1992**, *358*, 48−51.
(56) Mazaheri, M.; Razavi Hesabi, Z.; Sadrnezhaad, S. K. Two-Step Sintering of Titania Nanoceramics Assisted by Anatase-to-Rutile Phase Transformation. *Scr. Mater.* **2008**, *59*, 139−142.
(57) Gribb, A. A.; Banfield, J. F. Particle Size Effects on Transformation Kinetics and Phase Stability in Nanocrystalline TiO_2. *Am. Mineral.* **1997**, *82*, 717−728.
(58) Zhang, H. Z.; Banfield, J. F. New Kinetic Model for the Nanocrystalline Anatase-to-Rutile Transformation Revealing Rate Dependence on Number of Particles. *Am. Mineral.* **1999**, *84*, 528−535.
(59) Penn, R. L.; Banfield, J. F. Formation of Rutile Nuclei at Anatase {112} Twin Interfaces and the Phase Transformation Mechanism in Nanocrystalline Titania. *Am. Mineral.* **1999**, *84*, 871−876.
(60) Zhang, H. Z.; Banfield, J. F. Size Dependence of the Kinetic Rate Constant for Phase Transformation in TiO_2 Nanoparticles. *Chem. Mater.* **2005**, *17*, 3421−3425.
(61) Zhang, H. Z.; Banfield, J. F. Phase Transformation of Nanocrystalline Anatase-to-Rutile Via Combined Interface and Surface Nucleation. *J. Mater. Res.* **2000**, *15*, 437−448.
(62) Zhang, H. Z.; Banfield, J. F. Understanding Polymorphic Phase Transformation Behavior During Growth of Nanocrystalline Aggregates: Insights from TiO_2. *J. Phys. Chem. B* **2000**, *104*, 3481−3487.
(63) Lee, G. H.; Zuo, J.-M. Growth and Phase Transformation of Nanometer-Sized Titanium Oxide Powders Produced by the Precipitation Method. *J. Am. Ceram. Soc.* **2004**, *87*, 473−479.
(64) Ahn, J.-P.; Park, J.-K.; Kim, G. Effect of Compact Density on Phase Transition Kinetics from Anatase Phase to Rutile Phase During Sintering of Ultrafine Titania Powder Compacts. *Nanostruct. Mater.* **1998**, *10*, 1087−1096.
(65) Zhang, H. Z.; Banfield, J. F. Polymorphic Transformations and Particle Coarsening in Nanocrystalline Titania Ceramic Powders and Membranes. *J. Phys. Chem. C* **2007**, *111*, 6621−6629.
(66) Zhou, Y.; Fichthorn, K. A. Microscopic View of Nucleation in the Anatase-to-Rutile Transformation. *J. Phys. Chem. C* **2012**, *116*, 8314−8321.
(67) Zhou, J. F.; Zhou, M. F.; Caruso, R. A. Agarose Template for the Fabrication of Macroporous Metal Oxide Structures. *Langmuir* **2006**, *22*, 3332−3336.
(68) Lowell, S.; Shields, J. E.; Thomas, M. A.; Thommes, M. *Characterization of Porous Solids and Powders: Surface Area, Pore Size and Density*; Kluwer: London, 2004.